

Thermal Conductivity of the Accidental Degeneracy and Enlarged Symmetry Group Models for Superconducting UPt₃

M. J. Graf^{1,2}, S.-K. Yip¹ and J. A. Sauls¹

¹*Department of Physics & Astronomy, Northwestern University,
Evanston, Illinois 60208-3112*

²*Center for Materials Science, Los Alamos National Laboratory,
Los Alamos, New Mexico 87545*

(submitted in July 1998)

We present theoretical calculations of the thermal conductivity for the “accidental degeneracy” and “enlarged symmetry group” models that have been proposed to explain the phase diagram of UPt₃. The order parameters for these models possess point nodes or cross nodes, reflecting the broken symmetries of the ground state. These broken symmetries lead to robust predictions for the ratio of the low-temperature thermal conductivity for heat flow along the \hat{c} axis and in the basal plane. The anisotropy of the heat current response at low temperatures is determined by the phase space for scattering by impurities. The measured anisotropy ratio, κ_c/κ_b , provides a strong constraint of theoretical models for the ground state order parameter. The accidental degeneracy and enlarged symmetry group models based on no spin-orbit coupling do not account for the thermal conductivity of UPt₃. The models for the order parameter that fit the experimental data for the \hat{c} and \hat{b} directions of the heat current are the 2D E_{1g} and E_{2u} models, for which the order parameters possess line nodes in the ab-plane and point nodes along the \hat{c} axis, and the A_{1g} \oplus E_{1g} model of Zhitomirsky and Ueda. This model spontaneously breaks rotational symmetry in the ab-plane below T_{c2} and predicts a large anisotropy for the ab-plane heat current.

The observations of multiple superconducting phases^{1, 2, 3, 4} of UPt₃ have led to several Ginzburg-Landau models based on different symmetry groups or symmetry breaking scenarios in order to account for the phase diagram. In this paper we show that these models for the phase diagram, which are based on different pairing symmetries, lead to qualitatively different predictions for the thermal conductivity at very low temperatures.

The pairing models of UPt₃ which account for the main features of the phase diagram may be grouped into three classes. One class of models is based on a two-dimensional representation of D_{6h} with the multicomponent superconducting order parameter coupled to a *Symmetry-Breaking-Field (SBF)*. The leading candidates for the pairing state are the even-parity E_{1g} model and the odd-parity E_{2u} model. Both models require a symmetry breaking field in order to split the transition in zero field and produce multiple superconducting phases in a field. The *SBF* is generally assumed to be the in-plane AFM order parameter that onsets at $T_N \simeq 5\text{ K}$,⁶ however, other explanations of the *SBF* have been suggested.^{7, 8, 9}

Several authors have argued that the apparent tetracritical point in the H-T phase diagram for field orientations out of the basal plane is incompatible with the 2D E-rep models.^{10, 11, 12, 13} This led to explanations of the phase diagram in terms of multiple order parameters that are unrelated by symmetry (*e.g.* ‘AB-models’),^{10, 11} as well as further examination of the E-rep models.^{14, 15} The four possible E-rep models are not equivalent; weak hexagonal anisotropy, as is reflected by the weak in-plane anisotropy of H_{c2} ,^{16, 17} allows for an apparent tetracritical point for all field orientations provided the order parameter belongs to an E_2 orbital representation.¹⁴ The odd-parity, E_{2u} representation with strong spin-orbit locking of the order parameter with $\mathbf{d} \parallel \hat{\mathbf{c}}$ (\mathbf{d} is the quantization axis along which the pairs have zero spin projection, *i.e.* $\mathbf{d} \cdot \mathbf{S} = 0$) also accounts for the anisotropic paramagnetic limiting of H_{c2} observed at low temperatures.^{16, 18} The spin-singlet E_{1g} model appears to be incompatible with both the tetracritical point for $\mathbf{H} \not\perp \hat{\mathbf{c}}$ and the anisotropic Pauli limit for H_{c2} . However, Park and Joynt¹⁵ argue that there is enough freedom in the E_{1g} model to account for all existing experimental data. Analysis of current heat transport data at low temperatures is accounted for equally well by either E-rep. We suggest below that ultra-low temperature measurements of the thermal conductivity for varying impurity concentrations can also differentiate between the two E-rep models. Both E-rep models have recently been challenged by the observation of a nearly temperature independent Knight shift for $\mathbf{H} \parallel \hat{\mathbf{c}}$.¹⁹ Tou and co-workers¹⁹ favor the *ESG*-model of Machida *et al.*¹³ based on spin-triplet pairing with weak spin-orbit coupling. Thus, our current understanding of the spin structure and parity of the order parameter for UPt₃ is unclear because there is con-

flicting information from the NMR measurements of the spin susceptibility and measurements of the anisotropic paramagnetic limit of the upper critical field. However, as we show below, the low temperature thermal conductivity of UPt_3 is in strong conflict with the non-unitary spin-triplet model of Machida *et al.*¹³

The *AB*-models are based on an assumed near accidental degeneracy of two different pairing channels which are unrelated by symmetry.^{10,11} In these models the phase diagram is accounted for by *two* primary order parameters belonging to different irreducible representations of D_{6h} , which are selected in order to enforce a tetracritical point in the GL theory for the H-T phase diagram. The accidental degeneracy models which have been investigated in most detail assume that the two order parameters belong to different one-dimensional representations of the same parity, *e.g.* A_{2u} and B_{1u} .¹¹ Another group of models for the phase diagram may be described as *Enlarged-Symmetry-Group* models. These are hybrids of the accidental degeneracy and *SBF* models. The *ESG*-models assume an accidental degeneracy in the form of a “hidden symmetry”, which is lifted by a weak *SBF* coupling, similar to that of the *E*-rep models. Two different *ESG*-models have been proposed.^{13,20,21} The model of Zhitomirsky and Ueda²¹ is based on an enlarged *orbital* symmetry group for UPt_3 . In this model the primary pairing channel is assumed to be the *d*-wave ($\ell = 2$) channel of the full rotation group, and the degeneracy of the *d*-wave manifold is lifted by weak hexagonal anisotropy: $\Gamma_2[SO(3)] \rightarrow A_{1g} \oplus E_{1g} \oplus E_{2g}$. The A_{1g} and E_{1g} channels are assumed to be weakly split, in order to account for the double transition. Another formulation of an *ESG*-model assumes spin-triplet pairing with independent spin and orbital rotation symmetry, *i.e.* *no* spin-orbit coupling.¹³ In the model by Machida *et al.*¹³ a one-dimensional, odd-parity orbital representation is chosen in order to enforce a tetracritical point for all field orientations. The multicomponent order parameter corresponds to the three spin-triplet amplitudes described by the \mathbf{d} vector, and the *SBF* is assumed to be the AFM order parameter. The main features of each of these models of the phase diagram and thermodynamic quantities of UPt_3 are discussed in several articles.^{13,14,22,15}

In this paper we investigate the low-temperature transport properties for the ground states of the *AB* and *ESG* models. The heat transport coefficients are sensitive to the nodal structure and symmetry of the order parameter; at low temperatures the lower-dimensional regions of the Fermi surface associated with the nodal regions dominate the electronic heat transport. The nodes of $\Delta(\mathbf{p}_f)$ reflect the broken symmetries of the superconducting phase. The most specific information regarding the symmetry of the order parameter is reflected in the ultra-low temperature limit of the compo-

nents of the thermal conductivity tensor, *i.e.* $\lim_{T \rightarrow 0} \kappa/T$. The connection between the symmetry of the pairing state and the low temperature thermal conductivity is via impurity-induced Andreev scattering. Impurities in unconventional superconductors lead to a band of low-energy Fermion states which are formed by impurity-induced Andreev scattering and the momentum-space structure of the order parameter.²³ In a dilute alloy a distribution of impurities leads to a finite density of states, which we call an *Andreev band*. The bandwidth and density of states can be calculated from the self-consistent \hat{t} -matrix and the leading order impurity self-energy terms.^{40,24,25} Impurity scattering within the Andreev band is then the dominant heat transport mechanism at very low temperatures, *i.e.* $k_B T < \gamma$, where γ is the width of the Andreev band. The limiting values for κ/T are sensitive to the symmetry of the order parameter, the geometry and dimensionality of the nodes.^{25,5}

In an earlier paper⁵ we compared the electronic thermal conductivity measurements on UPt₃ by Lussier *et al.*²⁶ with our calculations based on the E-rep models. The experimental fact that $\kappa_c(T)/\kappa_c(T_c) < \kappa_b(T)/\kappa_b(T_c)$ for temperatures down to $T \simeq 50$ mK provides a strong constraint on models for the ground state order parameter and low-energy excitation spectrum. We found excellent agreement between theory and experiment for both the E_{1g} and E_{2u} representation [see also Norman and Hirschfeld²⁷ and Lussier *et al.*²⁶]. The quality of our fits for both E-rep models is evident in the temperature dependence of the normalized anisotropy ratio $[\kappa_c(T)/\kappa_b(T)]/(\kappa_c(T_c)/\kappa_b(T_c))$ (Figs. 2 and 3 of Ref. 5). From the published measurements, which extend down to $T_c/10$, it is not possible to distinguish between the low temperature phase of an even parity, spin singlet state (E_{1g}) and an odd parity, spin triplet pairing state (E_{2u}). Further experimental studies of the dependence of the anisotropy ratio on the impurity concentration are needed to distinguish between these two E-rep models. The differences in symmetry between the E_{1g} and E_{2u} models may be tested at ultralow temperatures on nearly clean materials. One possibility for distinguishing between the E_{1g} and E_{2u} ground states using transport measurements is based on the impurity scattering dependence of the asymptotic values of κ/T at temperatures below the impurity bandwidth, $k_B T \ll \gamma$. The predictions for the anisotropy ratio $\mathcal{R} = \lim_{T \rightarrow 0} [\kappa_c(T)/\kappa_b(T)]/[\kappa_c(T_c)/\kappa_b(T_c)]$ as a function of the normal-state impurity scattering rate are shown in Fig. 1 for the two E-rep models. The key feature is the universal (non-universal) limit for the E_{2u} (E_{1g}) model.

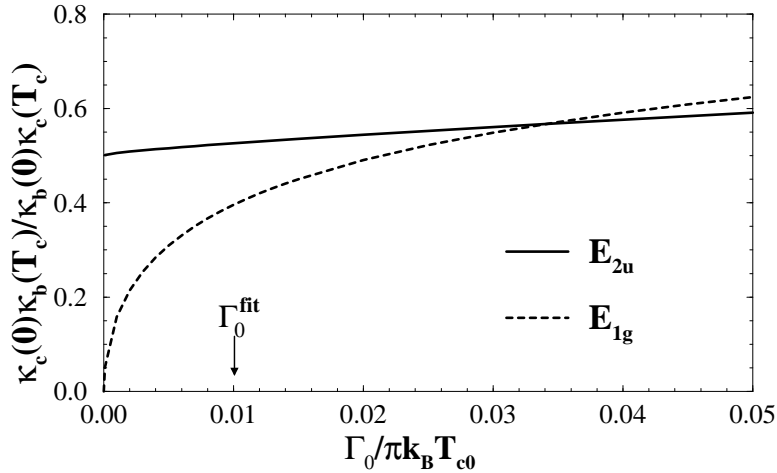


Fig. 1. The asymptotic low temperature anisotropy ratio of the thermal conductivities for an E_{1g} and E_{2u} order parameter with the ‘best fit’ parameters specified in Ref. (5). The arrow indicates the estimated scattering rate obtained from the data of Ref. (26) for the fit to the E_{2u} model.

Below we present our analysis of the electronic thermal conductivity for the representative ground states of the AB and ESG -models of UPt_3 . We discuss the variational forms for the order parameter of these models, and derive asymptotic limits for the low temperature thermal conductivity. We compare our analytical results for the asymptotic limits of κ/T with numerical calculations of the thermal conductivity over the full temperature range below T_c , and we compare the thermal conductivity calculated within the AB and ESG models with the experimental data on UPt_3 .^{26,45} None of the AB or ESG -models based on spin-triplet pairing without spin-orbit coupling account for the temperature dependence and anisotropy of the thermal conductivity at low temperatures. The only models which can account for the thermal conductivity data are the 2D E_{1g} and E_{2u} models, and the orbital ESG -model of Zhitomirsky and Ueda.²¹ The AE -model predicts a large *ab*-plane anisotropy, which differentiates it from the E-rep models. We discuss the conditions under which the AE -model can account for the heat transport data in UPt_3 .

Thermal Conductivity at Low Temperature

Our analysis focuses on the low temperature region, $T \lesssim 0.5 T_c$, where heat transport is limited by scattering of electronic quasiparticles off impurities. We consider *s*-wave scattering from a random distribution of defects in

the strong scattering limit ($\delta_0 \rightarrow \pi/2$). The assumption of nearly resonant scattering is in agreement with transport measurements in the normal Fermi-liquid and superconducting phases.²⁶ Inelastic “electron-electron” scattering is included by extrapolating the experimentally determined normal-state inelastic scattering rate, $1/\tau_{ee} = A T^2$, to temperatures below T_c ; inelastic scattering is negligible below $T \simeq 0.3T_c$.

The transport properties of unconventional superconductors are more strongly influenced by scattering from non-magnetic impurities than in conventional superconductors. One of the more striking effects is the appearance of a band of low energy excitations deep in the superconducting state.^{28,40,24,29,30} This occurs for non-magnetic impurities in unconventional superconductors when the order parameter changes sign around the Fermi surface. Impurity states develop from the combined effects of impurity scattering and Andreev scattering. In an unconventional superconductor with $\langle \Delta(\mathbf{p}_f) \rangle = 0$ and line or cross nodes, a finite concentration of impurities leads to Andreev states with a bandwidth, $\gamma \ll \Delta_0$, below which the density of states is non-zero and almost constant for $\epsilon < \gamma$.^{31,32} This novel metallic band, deep in the superconducting phase, can exhibit universal values for the transport coefficients, *i.e.* independent of the scattering rate at very low temperatures, $k_B T \ll \gamma$.^{33,34,35,25}

In Ref. [25] it was shown that the principal components of the thermal conductivity tensor can be expressed in terms of an *effective* transport scattering time that incorporates particle-hole coherence of the superconducting state. For $T \rightarrow 0$,

$$\lim_{T \rightarrow 0} \kappa_i(T) = \frac{v_{f,i}^2}{3} \gamma_S T \tau_i^{eff} \quad (i = a, b, c), \quad (1)$$

where $v_{f,i}^2$ is the Fermi-surface average of $[v_{f,i}(\mathbf{p}_f)]^2$, $\gamma_S = \frac{2}{3}\pi^2 k_B^2 N_f$ is the normal-state Sommerfeld coefficient, and

$$\tau_i^{eff} = \frac{3\hbar}{2v_{f,i}^2} \int d\mathbf{p}_f \frac{[v_{f,i}(\mathbf{p}_f)]^2 \gamma^2}{[\Delta(\mathbf{p}_f)^2 + \gamma^2]^{\frac{3}{2}}} \quad (2)$$

is the *effective* transport scattering time. The bandwidth of the Andreev states is given by

$$\gamma = \Gamma_u \frac{\langle \gamma (\Delta(\mathbf{p}_f)^2 + \gamma^2)^{-1/2} \rangle}{\cot^2 \delta_0 + \langle \gamma (\Delta(\mathbf{p}_f)^2 + \gamma^2)^{-1/2} \rangle^2}, \quad (3)$$

with the Fermi surface average $\langle \dots \rangle$, and $\Gamma_u = n_i/(\pi N_f)$. For a given impurity concentration, n_i , this bandwidth is largest in the limit of unitarity scattering, and depends on the order parameter symmetry through the structure and geometry of the nodes of $\Delta(\mathbf{p}_f)$ on the Fermi surface.

Order Parameter Models and Low Temperature Asymptotics

Earlier experimental^{36,37} and theoretical^{38,39,40,41,42} transport studies indicated that the excitation gap in UPt₃ has line nodes and probably polar point nodes. This is reinforced by the thermal conductivity data of Lussier *et al.*²⁶ which is fit almost perfectly down to $T \simeq 50$ mK by either the E_{1g} or the E_{2u} models, both of which have a line node in the *ab*-plane and polar point nodes. The differences in symmetry between the E_{1g} and E_{2u} states are predicted to show up in the impurity dependences of the anisotropy ratio $\lim_{T \rightarrow 0} \kappa_c/\kappa_b$ (see Fig. 1).⁵ However, as we show below the ground-state of the *AE*-model has cross nodes out of the basal plane located at polar angles, $\theta = \cos^{-1}(\pm 1/\sqrt{3})$. The *AE*-model can also account for the thermal conductivity data along the *c* and *b* axes. The model also predicts a large anisotropy in the *ab*-plane.

Table 1. Low temperature phases of several order parameter models. The first two entries are based on strong spin-orbit coupling and the symmetry group $[D_{6h}]_{\text{spin-orbit}} \times \mathcal{T} \times U(1)$. The third entry is based on no spin-orbit coupling and the *ESG*-subclass $SU(2)_{\text{spin}} \times [D_{6h}]_{\text{orbit}} \times \mathcal{T} \times U(1)$, and the last entry belongs to the mixed symmetry orbital subclass of the *ESG*, $SO(3)_{\text{spin-orbit}} \times \mathcal{T} \times U(1)$.

Γ	\mathcal{Y}_Γ	point	line	cross
E _{1g}	$z(x + iy)$	$\vartheta = 0, \pi$	$\vartheta = \frac{\pi}{2}$	—
E _{2u}	$\hat{\mathbf{c}}z(x + iy)^2$	$\vartheta = 0, \pi$	$\vartheta = \frac{\pi}{2}$	—
B _{1u}	$\mathbf{d} \operatorname{Im} (x + iy)^3$	$\vartheta_m = m\pi$ $m = 0, 1$	$\varphi_n = n\frac{\pi}{3}$, $n = 0, \dots, 5$	$\vartheta_m \wedge \varphi_n$
A _{2u} \oplus B _{1u}	$\hat{\mathbf{c}}[\mathbf{A} z \operatorname{Im} (x + iy)^6 + i \mathbf{B} \operatorname{Im} (x + iy)^3]$	$\vartheta_m = m\pi$ $m = 0, 1$	$\varphi_n = n\frac{\pi}{3}$, $n = 0, \dots, 5$	$\vartheta_m \wedge \varphi_n$
A _{1g} \oplus E _{1g}	$\mathbf{A} (2z^2 - x^2 - y^2)$ + $i \mathbf{E} yz$	—	—	$\vartheta = \cos^{-1} \frac{\pm 1}{\sqrt{3}}$ $\wedge \varphi = 0, \pi$

Generic basis functions⁴³ for E-rep models, *AB* and *ESG*-models for the ground state of UPt₃ are listed in Table 1. All of these models have both line nodes and point nodes - or “cross nodes” which are point nodes formed at the intersection of line nodes in the two different basis functions

of the accidental degeneracy models. Order parameter models like the polar state (A_{1u}), or combinations of the polar state with a nodeless A_{1g} state are excluded by existing transport data.

Crystal symmetry alone does not determine the detailed structure of the order parameter or excitation gap as a function of position on the Fermi surface. In particular, the behavior of $\Delta(\mathbf{p}_f)$ in the vicinity of the nodes depends on material parameters. These ‘nodal’ parameters determine the rate at which the excitation gap opens near a linear point or line node (*e.g.* E_{1g} ground state), the curvature of a quadratic point node (*e.g.* E_{2u} ground state) or the third derivative of a cubic point node (*e.g.* B_{1u} state). In principle these nodal parameters can be calculated by solving for the eigenfunctions of the linearized gap equation, but this requires precise knowledge of the pairing interaction for momenta on the Fermi surface. Our approach is to enforce the symmetry of $\Delta(\mathbf{p}_f)$ through the positions of the nodes and to model the nodal structure with phenomenological parameters which we fix by comparison with experiment. Variational basis functions are constructed from the generic basis functions by multiplying by a function, \mathcal{F}_Γ , which is invariant under all crystal group operations. This procedure allows us to introduce the Fermi surface anisotropy into the basis functions and independently model the nodal regions of the excitation spectrum for line and point nodes. Although the specific choice of functions \mathcal{F}_Γ for a given representation is not unique, once we fix the nodal parameters the low temperature thermal conductivity is determined. As we have shown previously,^{25,5} the low-temperature response is dominated by the lower dimensional regions of the Fermi surface near the nodes of the order parameter; in these regions impurity induced Andreev states with energies $\epsilon < \gamma \ll \Delta_0$ form a ‘metallic’ band that determines the transport properties at $k_B T < \gamma$.

A key feature required to account for heat transport in UPt_3 is the existence of gapless excitations with both $\mathbf{v}_f \cdot \hat{\mathbf{c}} \neq 0$ and $\mathbf{v}_f \cdot \hat{\mathbf{b}} \neq 0$. Machida *et al.*¹³ proposed an *ESG*-model based on no spin-orbit coupling and a 3D order parameter in spin space, corresponding to the three possible spin-triplet pair states, all of which have the same orbital pair wave function. They assume a 1D orbital function with A_{2u} or B_{1u} symmetry.¹³ The corresponding orbital basis functions are

$$\Delta^{A_{2u}}(\mathbf{p}_f) = \left[\Delta_0^A(T) \frac{343\sqrt{7}}{216} \hat{p}_z \text{Im}(\hat{p}_x + i\hat{p}_y)^6 \right] \mathcal{F}_{A_{2u}}(\mathbf{p}_f; \mu, \mu_6), \quad (4)$$

$$\Delta^{B_{1u}}(\mathbf{p}_f) = \left[\Delta_0^B(T) \text{Im}(\hat{p}_x + i\hat{p}_y)^3 \right] \mathcal{F}_{B_{1u}}(\mathbf{p}_f; \mu, \mu_3), \quad (5)$$

with $\Delta(\theta) \approx \Delta_0 \mu_n \theta^n$ near the point node, and $\Delta(\theta) \approx \Delta_0 \mu \phi$ near the line node at $\phi = 0$. The B_{1u} function has a cubic point and three *axial* line

nodes. The distinctive feature of this model is the large density of low-energy excitations near the poles. The A_{2u} function has a sixth-order point node and six axial line nodes. Among the AB -models, the $A_{2u} \oplus B_{1u}$ order parameter, $\Delta^{AB}(\mathbf{p}_f) = \Delta^{A_{2u}}(\mathbf{p}_f) + i\Delta^{B_{1u}}(\mathbf{p}_f)$, has the same nodal features as the B_{1u} model, *i.e.* a cubic point node and three axial line nodes.

The density of impurity-induced Andreev states near the point and line nodes, and the heat current carried by these states, depends sensitively on the gap function near the point or line nodes. For a cubic point node at the poles, $\Delta(\phi = \pi/6, \theta) \approx \mu_3 \Delta_0 \theta^3$, which leads to $\kappa_c/T \sim \mu_3^{-2/3}$ as $T \rightarrow 0$.²⁵ Thus, increasing μ_3 tends to reduce the phase space for scattering among states near the cubic point node (see Fig. 2). This is the case for both B_{1u} and $A_{2u} \oplus B_{1u}$ models provided $\mu_3 < 1$.

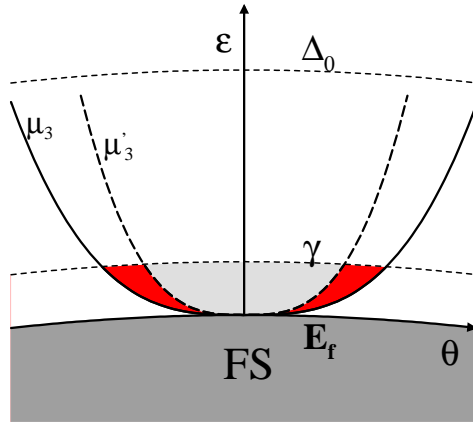


Fig. 2. The gap function $|\Delta(\theta)| \approx \mu_3 \Delta_0 |\theta|^3$ at the Fermi surface (FS) near a cubic point node. At low temperatures $T \lesssim \gamma \ll \Delta_0$ the excitations are confined to a lower dimensional region of the Fermi surface, *i.e.* $0 \leq \epsilon \lesssim \gamma$ near the node. The solid (dashed) line corresponds to a gap function with nodal parameter μ_3 (μ'_3). The dark shaded area is a measure of the increase in phase space for $\mu_3 < \mu'_3$.

For $\mu_3 \lesssim 1$ the low temperature limit of the anisotropy ratio of the thermal conductivity for the B_{1u} state is,²⁵

$$\mathcal{R} \equiv \frac{\kappa_c(0)/\kappa_b(0)}{\kappa_c(T_c)/\kappa_b(T_c)} \sim 10 \frac{\mu}{\mu_3} \left(\frac{\mu_3 \Delta_0}{\gamma} \right)^{1/3}, \quad (6)$$

where μ is the nodal parameter for the axial line nodes, *i.e.* $\Delta(\phi, \theta = \pi/2) \approx \mu \Delta_0 \phi$. For $\mu_3 \sim 1$ and $\gamma/\Delta_0 \ll 1$ the ratio is typically much larger than unity. Based on Eq.(6) it appears possible to accommodate the experimental constraint, $\mathcal{R}_{\text{expt}} < 1$, with a B_{1u} order parameter by increasing μ_3 , *i.e.*

decreasing the phase space associated from the cubic point node.²⁵ However, Eq. (6) breaks down for $\mu_3 > 1$. This corresponds to shrinking and effectively removing the cubic point nodes. In this limit the axial line nodes determine the transport coefficients for both the *c*-axis and *ab*-plane currents. We find that $\mathcal{R} \geq 1$, and in the limit $\mu_3 \gg 1$ the anisotropy ratio approaches unity (see also Table 2).

The result $\mathcal{R} \geq 1$ also applies to the *AB*-model. This can be understood by noting that in the calculation of the thermal conductivity the order parameter enters as $\Delta\Delta^*$. For the $A_{2u} \oplus B_{1u}$ order parameter the product $\Delta\Delta^* = |\Delta^{A_{2u}}(\mathbf{p}_f) + i\Delta^{B_{1u}}(\mathbf{p}_f)|^2$ can always be written in the form $|\Delta^{B_{1u}}(\mathbf{p}_f)|^2(1 + \mathcal{F}(\mathbf{p}_f))$, where \mathcal{F} is an invariant function. This is precisely the variational form for the product for the basis function with B_{1u} symmetry discussed above. Thus, we conclude that the $A_{2u} \oplus B_{1u}$ model cannot accommodate the experimental result $\mathcal{R}_{\text{expt}} < 1$. The same arguments can be applied to the other relevant order parameter models of the *AB*-class, e.g. $A_{1u} \oplus B_{1u}$ and $A_{1g} \oplus B_{2g}$. Thus, for a unitary order parameter belonging to the spin version of the *ESG*-models (e.g. B_{1u}), and for the same parity subclasses of the *AB*-models, e.g. $A_{2u} \oplus B_{1u}$, the anisotropy ratio is always greater than unity, which disagrees with the experimental results for \mathcal{R} .²⁶

Table 2. Asymptotic values of the thermal conductivity tensor κ/T for $T \rightarrow 0$.

Rep		$\kappa_b(T) \left(\frac{1}{2} \gamma_S T v_{f,b}^2 \right)^{-1}$	$\kappa_c(T) \left(\frac{1}{2} \gamma_S T v_{f,c}^2 \right)^{-1}$
E_{1g}	$\mu_1 \sim 1$	$1/(2\mu\Delta_0)$	$\gamma/(\mu_1^2\Delta_0^2)$
E_{2u}	$\mu_2 \sim 1$	$1/(2\mu\Delta_0)$	$1/(2\mu_2\Delta_0)$
B_{1u}	$\mu_3 \sim 1$	$3/(2\mu\Delta_0)$	$\frac{\sim 1}{\mu_3\Delta_0} (\mu_3\Delta_0/\gamma)^{\frac{1}{3}}$
	$\mu_3 \gg 1$	$2/(\pi\mu\Delta_0)$	$2/(\pi\mu\Delta_0)$
$A_{2u} \oplus B_{1u}$	$\mu_3 \sim 1$	$3/(2\mu\Delta_0^{B_{1u}})$	$\frac{\sim 1}{\mu_3\Delta_0^{B_{1u}}} (\mu_3\Delta_0^{B_{1u}}/\gamma)^{\frac{1}{3}}$
	$\mu_3 \gg 1$	$2/(\pi\mu\Delta_0^{B_{1u}})$	$2/(\pi\mu\Delta_0^{B_{1u}})$
$A_{1g} \oplus E_{1g}$	$\mu_A, \mu_E \sim 1$	$\frac{\sim \gamma^3}{(\mu_A\Delta_0^A) (\mu_E\Delta_0^E)^3}$	$\frac{\sim \gamma}{(\mu_A\Delta_0^A) (\mu_E\Delta_0^E)}$

Machida *et al.*^{13,44} argue that UPt_3 is described by a non-unitary spin-triplet ground state. Non-unitary ground states break time-reversal symmetry in spin space; $\mathbf{S}(\mathbf{p}_f) = i\Delta(\mathbf{p}_f) \times \Delta^*(\mathbf{p}_f)$ is proportional to

the spin polarization of triplet pairs with relative momenta \mathbf{p}_f . The ground state of the *ESG*-model of Ref. (13, 44) is a non-unitary state with $\Delta = \Delta(\mathbf{p}_f)(\hat{\mathbf{a}} + i\hat{\mathbf{c}})/2$. The corresponding excitation spectrum has two branches: $E_\uparrow = \sqrt{\xi_{\mathbf{p}_f}^2 + |\Delta(\mathbf{p}_f)|^2}$ and $E_\downarrow = |\xi_{\mathbf{p}_f}|$, where \uparrow (\downarrow) corresponds to an excitation with spin parallel (anti-parallel) to \mathbf{S} . Thus, the down-spin excitations are gapless over the whole Fermi surface and give rise to a large heat current at low temperatures compared to unitary or even parity superconducting states. The low temperature thermal conductivity is greater than half the normal-state value extrapolated below T_c , i.e. $\kappa/T \geq \frac{1}{2}\kappa_N/T$. From Ref. (26) we deduce that the normal-state scattering rate extrapolated to $T = 0$ is $1/\tau(0) \approx \frac{1}{2} \times 1/\tau(T_c)$. This gives $\lim_{T \rightarrow 0} \kappa/T \gtrsim [\kappa_N/T]_{T_c}$, a result which is in striking contrast with the low temperature experimental data for UPt_3 , which are roughly two orders of magnitude smaller, i.e. $\lim_{T \rightarrow 0} \kappa_i/T \sim 0.01[\kappa_i/T]_{T_c}$, with $i = a, c$. Thus, a non-unitary ground state of the form proposed by Machida *et al.*^{13, 44} is incompatible with the thermal conductivity data on UPt_3 .¹

Now consider the orbital *ESG*-model proposed by Zhitomirsky and Ueda.²¹ They start from the five-dimensional $\ell = 2$ orbital representation of the full rotation group and assume that crystal-field terms break the full rotational symmetry and split the d-wave representation into three irreducible representations of D_{6h} ; $\Gamma_2[SO(3)] \Rightarrow A_{1g} \oplus E_{1g} \oplus E_{2g}$ with $T_c^{A_{1g}} > T_c^{E_{1g}} \gg T_c^{E_{2g}}$. The onset of superconductivity is identified with the A_{1g} component, and the second transition is identified with nucleation of an E_{1g} component. The *AE*-model would in principle predict a third transition involving the E_{2g} amplitude, however, no such transition is observed in UPt_3 . Thus, $T_c^{E_{2g}}$ must be suppressed to very low temperatures by the development of the first two order parameter components.

The onset of an E_{1g} order parameter spontaneously breaks both time-reversal symmetry and rotational symmetry in the basal plane. The ground-state order parameter in the *AE*-model has the form, $\Delta^{AE}(\mathbf{p}_f) = \Delta^{A_{1g}}(\mathbf{p}_f) + i\Delta^{E_{1g}}(\mathbf{p}_f)$, with possible basis functions

$$\Delta^{A_{1g}}(\mathbf{p}_f) = \left[\Delta_0^A(T) \frac{1}{2}(3\cos(\theta)^2 - 1) \right] \mathcal{F}_{A_{1g}}(\mathbf{p}_f; \mu_A), \quad (7)$$

$$\Delta^{E_{1g}}(\mathbf{p}_f) = \left[\Delta_0^E(T) \sin(2\theta) \sin(\phi) \right] \mathcal{F}_{E_{1g}}(\mathbf{p}_f; \mu_E). \quad (8)$$

The A_{1g} basis function has tropical line nodes above and below the equator at $\theta = \cos^{-1}(\pm 1/\sqrt{3})$. The E_{1g} basis function has an axial line node run-

¹ Early transport and heat capacity experiments at higher temperatures on poorer quality crystals were interpreted in terms of a large residual density of states at the Fermi energy. Indeed this interpretation was the original argument for introducing the non-unitary spin-triplet pairing model for UPt_3 .

ning from the north pole to the south pole. Consequently the ground-state *AE* order parameter has four cross nodes located at the intersection of the tropical and axial line nodes. As can be seen from Table 2 the asymptotic values of the thermal conductivities of the *AE*-model are nonuniversal.²

An additional feature of the *AE*-model is that the low-temperature phase spontaneously breaks rotational symmetry in the *ab*-plane. The low-temperature phase of the Ginzburg-Landau (GL) functional for the *AE*-model is also degenerate with respect to rotations of the E_{1g} order parameter in the *ab*-plane. This accidental degeneracy is lifted by higher order terms in the free energy (sixth-order and higher) which differentiate hexagonal symmetry from cylindrical symmetry. In order for the *AE*-model to account for the thermal conductivity data for heat flow along the *c* and *b* axes the ground-state must *orient* such that the axial line node of the E_{1g} order parameter is along the *a*-direction (k_x -direction). If the hexagonal anisotropy energy is small, $\mathcal{F}_{hex} \ll N_f |\Delta|^2$, the heat current may orient the E_{1g} order parameter so that the current response is nearly isotropic in the *ab*-plane. However, for sufficiently small currents the anisotropy of the thermal conductivity tensor that results from the spontaneously broken rotational symmetry in the *ab*-plane should be observable. Table 2 summarizes the low temperature limits for the thermal conductivities for the models discussed above.

Numerical Results and Conclusions

In order to obtain quantitative results for the thermal conductivity over the full temperature range below T_c we must include inelastic ‘electron-electron’ scattering. We model the inelastic scattering rate in the superconducting phase of UPt₃ by extrapolating the normal-state scattering rate, $1/\tau_{ee} = AT^2$, below T_c . For $T \lesssim 0.3T_c$ the inelastic channel is unimportant even for the clean limit of UPt₃ discussed here. The combined elastic and inelastic scattering rate in the normal-state is $\Gamma(T) = \Gamma_0 + AT^2$. From the measurements in Ref. 26 it follows that the UPt₃ crystals that were studied have nearly equal elastic and inelastic scattering rates at T_c , i.e. $\Gamma_0 = AT_c^2$, so that $\Gamma(T) = \Gamma_0(1 + T^2/T_c^2)$. Our procedure for computing and fitting the thermal conductivities is described in detail in Refs. 25 and 5. Below T_c we assume that the elastic scattering is in the unitarity limit.⁵ Here we briefly outline the procedure and then discuss the numerical results for the B_{1u} , AB , and *AE* models.

² An extra complication in the analysis of the *AE*-model is that the angular average of the order parameter is (generally) nonvanishing, $\langle \Delta^{A_{1g}}(\mathbf{p}_f) \rangle \neq 0$, which results in nonvanishing off-diagonal contributions to the scattering self-energy which must be calculated self-consistently.

We describe the analysis of the B_{1u} order parameter; a similar analysis is carried out for the other order parameter models. We first calculate the basal plane thermal conductivity, κ_b , and adjust the scattering rate Γ_0 and the nodal parameters, μ at $\phi = 0, \theta = \pi/2$ and μ_3 at $\phi = \pi/6, \theta = 0$, to obtain a good fit between theory and experiment. The next step is to compute κ_b and κ_c keeping Γ_0 and μ fixed, and relaxing μ_3 for a best fit. Figure 3 shows the nearly perfect fit to the basal plane thermal conductivity of Ref. (26) for the B_{1u} model.

For the variational function $\mathcal{F}_{B_{1u}}$ we have chosen the form

$$\mathcal{F}_{B_{1u}} = y_0(a_\phi, a_\theta) \left(1 + a_\phi \cos^2(3\phi) + a_\theta \cos^2(\theta) \right), \quad (9)$$

where the prefactor y_0 is determined by $\max \Delta(\mathbf{p}_f) = \Delta_0$. The coefficients (a_ϕ, a_θ) determine the nodal parameters,

$$\mu = 3(1 + a_\phi) y_0(a_\phi, a_\theta), \quad (10)$$

$$\mu_3 = (1 + a_\theta) y_0(a_\phi, a_\theta). \quad (11)$$

Thus, we have two variational parameters (a_ϕ, a_θ) that enable us to independently adjust the nodal parameters μ and μ_3 .

We also examined the sensitivity of our numerical results to the form of the variational function. In particular, we calculated the thermal conductivity for a piecewise continuous B_{1u} order parameter of the form $\Delta(\phi, \theta) = \Delta_0^{B_{1u}} g(\phi)h(\theta)$ with

$$g(\phi) = \begin{cases} \mu \Delta_0 \phi & : 0 \leq \phi < \phi_*, \\ 1 & : \phi_* \leq \phi \leq \frac{\pi}{6}, \end{cases} \quad (12)$$

$$h(\theta) = \begin{cases} \mu_3 \Delta_0 \theta^3 & : 0 \leq \theta < \theta_*, \\ 1 & : \theta_* \leq \theta \leq \frac{\pi}{2}, \end{cases} \quad (13)$$

where $\phi_* = \min(\frac{\pi}{6}, 1/\mu \Delta_0)$, and $\theta_* = \min(\frac{\pi}{2}, 1/(\mu_3 \Delta_0)^{1/3})$, and the imposed B_{1u} symmetry on the functions $g(\phi)h(\theta)$; i.e. $g(\frac{\pi}{3} - \phi) = g(\phi)$, $g(\frac{\pi}{3} + \phi) = -g(\phi)$, and $h(\pi - \theta) = h(\theta)$.

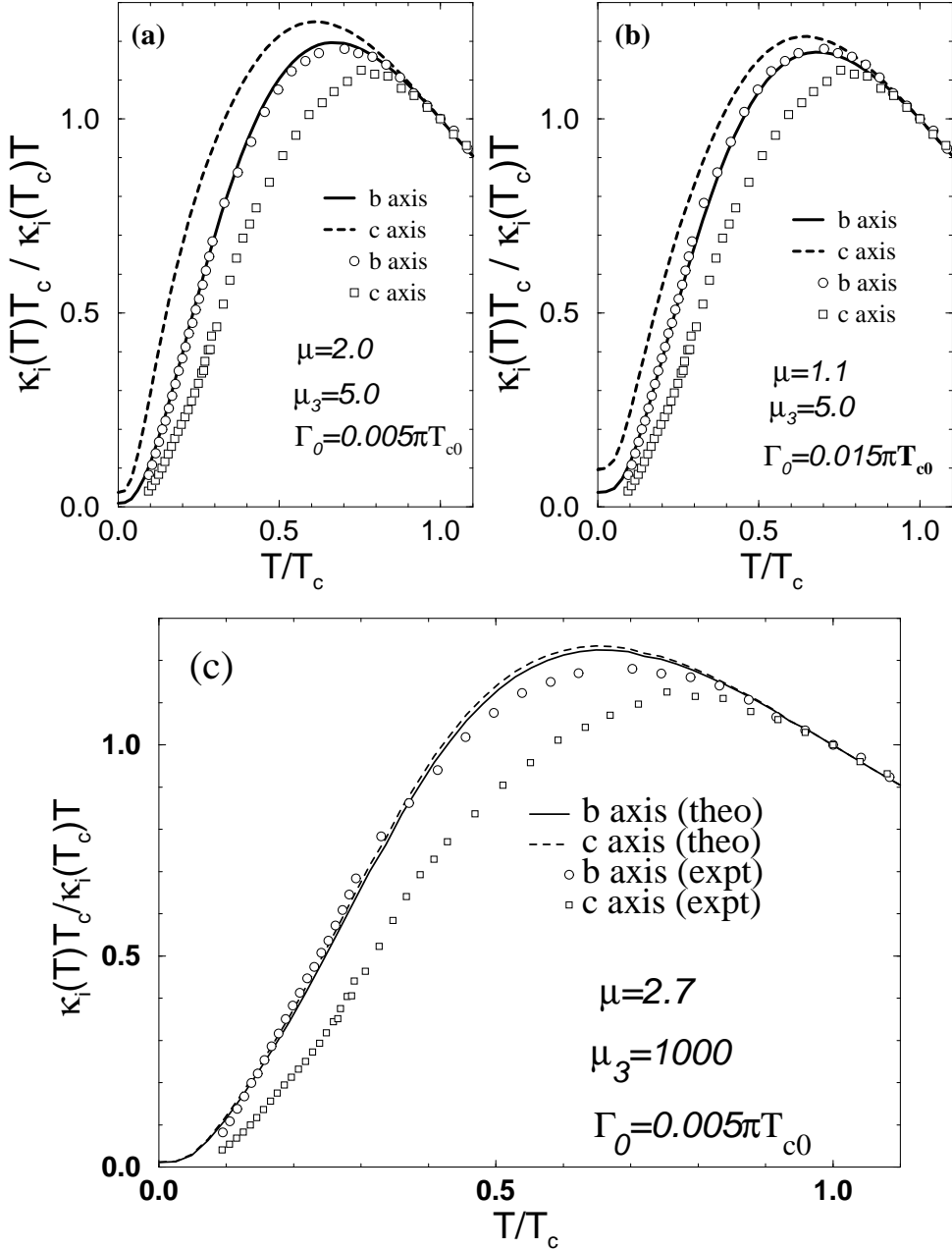


Fig. 3. (a) The normalized thermal conductivities for a B_{1u} state in comparison with the experimental data on UPt_3 .²⁶ The best fit parameters are shown in the figure. (b) The same comparison for the $A_{2u} \oplus B_{1u}$ model, and (c) for a piecewise continuous B_{1u} state (see text).

With this piecewise B_{1u} model we confirm our earlier conclusions, *viz.* that only the values of Δ_0 , Γ_0 , and $\{\mu_i\}$ vary slightly, but the best fit low-temperature thermal response functions are unaffected. Furthermore, in the limit $\mu_3 \gg 1$ (ie. $h(\theta) \rightarrow 1$) we obtain $\mathcal{R} \rightarrow 1$ for the asymptotic anisotropy ratio (see Fig. 3c). In short, all the numerical results are in agreement with our estimates of the asymptotic values of the B_{1u} pair state. These considerations apply to the analysis of the AB and ESG -models as well.

Figure 3 shows our ‘best fit’ calculations for the B_{1u} (Fig. 3a) and AB (Fig. 3b) order parameter models. For both models we obtain excellent fits to the basal plane thermal conductivity, κ_b/T , over the entire temperature range. However, we are unable to fit the c -axis thermal conductivity with the B_{1u} and AB order parameter models, which is consistent with our phase space arguments and asymptotic estimates.

We obtain good low temperature fits for both the b and c axis thermal conductivity with the AE -model provided the E_{1g} component is oriented with the axial line node along the a -axis. The insert in Fig. 4 shows the strong anisotropy of the heat flow in the ab -plane for the AE -model, *i.e.* $\lim_{T \rightarrow 0} \kappa_a/\kappa_b \sim 4$, which is a direct consequence of the broken rotational symmetry in the basal plane. This anisotropy, which is specific to the AE -model, has not been experimentally observed. It would serve as an important test of the AE -model and would differentiate the model from the $2D$ E-*rep* models. The nodal parameters, which determine the spectrum of low-lying excitations around the cross nodes, are defined as $\Delta^{A_{1g}}(\theta) \approx \Delta_0^A \mu_A(\theta_* - \theta)$, with $\theta_* = \cos^{-1} \sqrt{1/3}$, and $\Delta^{E_{1g}}(\phi) \approx \Delta_0^E \mu_E \phi$.

The quality of our fits for the thermal conductivity along different crystal axes is best summarized in terms of the anisotropy ratios $\mathcal{R}(T) = [\kappa_c(T)/\kappa_b(T)]/(\kappa_c(T_c)/\kappa_b(T_c))$ for the various order parameter models. Figure 5 shows that the anisotropy ratio for the data of Ref. (26) is well described by the ground states for the E_{1g} , E_{2u} and $A_{1g} \oplus E_{1g}$ models. The AB -models, and the spin-triplet ESG -models cannot account for the anisotropy of the thermal conductivity at low temperatures.

Independent measurements of the thermal conductivity by Suderow *et al.*⁴⁵ differ somewhat from those of Lussier *et al.*,²⁶ particularly in the anisotropy ratio \mathcal{R} . This difference is mainly due to differences in the c -axis thermal conductivity. The normalized basal plane conductivities, plotted vs. T/T_c , are in remarkably good agreement, despite of being measured on different samples. The differences in the data for heat flow along the c -axis for the different samples might be due to crystal imperfections along the c -axis, such as stacking faults, structural modulations or a mosaic structure.

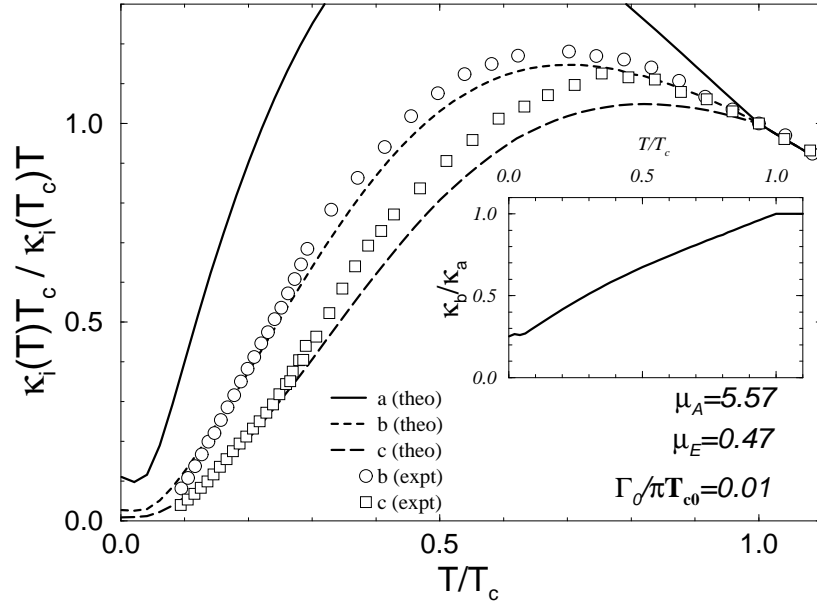


Fig. 4. The normalized thermal conductivities for the $A_{1g} \oplus E_{1g}$ model in comparison with the experimental data on UPt_3 .²⁶ The inset shows the ratio of the conductivities κ_b/κ_a .

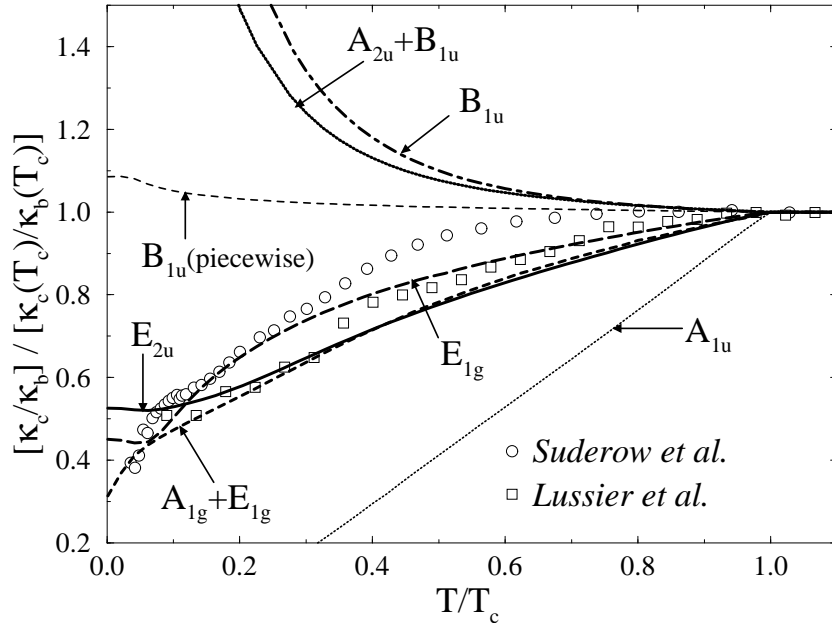


Fig. 5. The anisotropy ratio of the thermal conductivities for various ‘best fit’ pairing states. The lines for an E_{1g} , E_{2u} and A_{1u} state are shown for comparison.

Conclusion

Our analysis of the low temperature thermal conductivities for a single component order parameter of the *ESG*-class (*e.g.* B_{1u}), and the accidental degeneracy order parameter models of the *AB*-class (*e.g.* $A_{2u} \oplus B_{1u}$), and the orbital subclass of the *ESG*-class ($A_{1g} \oplus E_{1g}$), support earlier analyses suggesting that one of the *2D* E-rep models is a promising model for the order parameter of UPt_3 . The *AB*-models and the spin-triplet version of the *ESG*-model are in substantial disagreement with the experimental data at low temperatures. Cubic point nodes or cross nodes at or near the poles of the Fermi surface lead to a large heat current along the *c*-axis, which is not reconcilable with the experimental data. The two-component orbital *AE*-model can account for the *c*-axis and *b*-axis thermal conductivities with an appropriate orientation of the E_{1g} order parameter. However, the *AE*-model spontaneously breaks rotational symmetry in the basal plane which so far has not been observed in any experiment to date. The basal plane anisotropy is large ($\lim_{T \rightarrow 0} \kappa_a / \kappa_b \sim 4$) and should easily be detected.

Acknowledgments

This research was supported by the National Science Foundation (grant no. DMR-9705473) and the Science and Technology Center for Superconductivity (grant no. DMR 91-20000). MJG also acknowledges support from Los Alamos National Laboratory under the auspices of the U.S. Department of Energy, where this work was completed.

REFERENCES

1. V. Müller *et al.*, Phys. Rev. Lett. **58**, 1224 (1987).
2. Y. Qian *et al.*, Solid State Commun. **63**, 599 (1987).
3. G. Bruls *et al.*, Phys. Rev. Lett. **65**, 2294 (1990).
4. S. Adenwalla *et al.*, Phys. Rev. Lett. **65**, 2298 (1990).
5. M. J. Graf, S.-K. Yip, and J. A. Sauls, J. Low Temp. Phys. - Rapid Comm. **102**, 367 (1996); (E) **106**, 727 (1997).
6. S. Hayden, L. Taillefer, C. Vettier, and J. Flouquet, Phys. Rev. **B46**, 8675 (1992).
7. P. A. Midgley *et al.*, Phys. Rev. Lett. **70**, 678 (1993).
8. V. Mineev, Sov. Phys. JETP Lett. **57**, 683 (1993).
9. B. Ellman, A. Zahluska, and L. Taillefer, Physica B **205**, 346 (1995); B. Ellman, *et al.*, LANL E-print <http://xxx.lanl.gov/abs/cond-mat/9704125>.
10. I. Luk'yanchuk, J. de Phys. **I1**, 1155 (1991).
11. D. Chen and A. Garg, Phys. Rev. Lett. **70**, 1689 (1993).
12. K. Machida and M. Ozaki, Phys. Rev. Lett. **66**, 3293 (1991).

13. K. Machida, T. Ohmi, and M. Ozaki, *J. Phys. Soc. Jpn.* **62**, 3216 (1993).
14. J. Sauls, *Adv. Phys.* **43**, 113 (1994).
15. K. Park and R. Joynt, *Phys. Rev. B* **53**, 12346 (1996).
16. B. Shivaram, T. Rosenbaum, and D. Hinks, *Phys. Rev. Lett.* **57**, 1259 (1986).
17. N. Keller, J. L. Tholence, A. Huxley, and J. Flouquet, *Phys. Rev. Lett.* **73**, 2364 (1994).
18. C. Choi and J. Sauls, *Phys. Rev. Lett.* **66**, 484 (1991).
19. X. Tou and *et al.*, *Phys. Rev. Lett.* **80**, 3129 (1998).
20. M. Zhitomirskii and I. Luk'yanchuk, *Sov. Phys. JETP Lett.* **58**, 131 (1993).
21. M. Zhitomirskii and K. Ueda, *Phys. Rev. B* **53**, 6591 (1996).
22. R. Heffner and M. Norman, *Comm. Cond. Matt. Phys.* **17**, 361 (1996).
23. J. A. Sauls and D. Rainer, *Czech. J. Phys.* **47**, 1065 (1996).
24. C. Choi and P. Muzikar, *Phys. Rev. B* **36**, 54 (1987).
25. M. J. Graf, S.-K. Yip, J. A. Sauls, and D. Rainer, *Phys. Rev. B* **53**, 15147 (1996).
26. B. Lussier, B. Ellman, and L. Taillefer, *Phys. Rev. B* **53**, 5145 (1996).
27. M. Norman and P. Hirschfeld, *Phys. Rev. B* **53**, 5706 (1996).
28. L. J. Buchholtz and G. Zwicknagl, *Phys. Rev. B* **23**, 5788 (1981).
29. G. Preosti, H. Kim, and P. Muzikar, *Phys. Rev. B* **50**, 1259 (1994).
30. A. Balatsky, M. L. Salkola, and A. Rosengreen, *Phys. Rev. B* **51**, 15547 (1995).
31. L. Gor'kov and P. A. Kalugin, *Sov. Phys. JETP Lett.* **41**, 254 (1985).
32. C. Choi and P. Muzikar, *Phys. Rev. B* **37**, 5947 (1988).
33. M. Lee *et al.*, *Phys. Rev. B* **48**, 7392 (1993).
34. M. J. Graf, M. Palumbo, D. Rainer, and J. A. Sauls, *Phys. Rev. B* **52**, 10588 (1995).
35. Y. Sun and K. Maki, *Euro. Phys. Lett.* **32**, 355 (1995).
36. B. Shivaram, Y. Jeong, T. Rosenbaum, and D. Hinks, *Phys. Rev. Lett.* **56**, 1078 (1986).
37. C. Broholm *et al.*, *Phys. Rev. Lett.* **65**, 1078 (1990).
38. K. Miyake, S. Schmitt-Rink, and C. Varma, *Phys. Rev. B* **34**, 6554 (1986).
39. S. Schmitt-Rink, K. Miyake, and C. Varma, *Phys. Rev. Lett.* **57**, 2575 (1986).
40. P. J. Hirschfeld, D. Vollhardt, and P. Wölfle, *Sol. State Comm.* **59**, 111 (1986).
41. H. Monien, K. Scharnberg, L. Tewordt, and N. Schopohl, *J. Low Temp. Phys.* **65**, 13 (1986).
42. C. J. Pethick and D. Pines, *Phys. Rev. Lett.* **57**, 118 (1986).
43. S. Yip and A. Garg, *Phys. Rev. B* **48**, 3304 (1993).
44. K. Machida and T. Ohmi, *J. Phys. Soc. Jpn.* **67**, 1122 (1998).
45. H. Suderow, J. P. Brison, A. Huxley, and J. Flouquet, *J. Low Temp. Phys.* **108**, 11 (1997).